CLIMATE CHANGE AND WILDFIRE IN AND AROUND CALIFORNIA: FIRE MODELING AND LOSS MODELING

WHITE PAPER

DRAFT

A Report From:
California Climate Change Center

Prepared By:
Anthony Westerling
Benjamin Bryant

DISCLAIMER

Arnold Schwarzenegger, *Governor*

December 2005
CEC-500-2005-190-SD

Acknowledgements

We gratefully acknowledge our debt to Dr. Haiganoush Preisler, USDA Forest Service Pacific Southwest Research Station, and to Dr.'s Hugo Hidalgo and Alexander Gershunov, Scripps Institution of Oceanography, for their comments and advice, and to David Sapsis and Robin Marose of the California Department of Forestry and Fire Protection for their assistance with county assessor's parcel data. Any errors or omissions are our own.

Preface

The Public Interest Energy Research (PIER) Program supports public interest energy research and development that will help improve the quality of life in California by bringing environmentally safe, affordable, and reliable energy services and products to the marketplace.

The PIER Program, managed by the California Energy Commission (Energy Commission), annually awards up to $62 million to conduct the most promising public interest energy research by partnering with Research, Development, and Demonstration (RD&D) organizations, including individuals, businesses, utilities, and public or private research institutions.

PIER funding efforts are focused on the following RD&D program areas:

- Buildings End-Use Energy Efficiency
- Energy-Related Environmental Research
- Energy Systems Integration
- Environmentally Preferred Advanced Generation
- Industrial/Agricultural/Water End-Use Energy Efficiency
- Renewable Energy Technologies

The California Climate Change Center (CCCC) is sponsored by the PIER program and coordinated by its Energy-Related Environmental Research area. The Center is managed by the California Energy Commission, Scripps Institution of Oceanography at the University of California at San Diego, and the University of California at Berkeley. The Scripps Institution of Oceanography conducts and administers research on climate change detection, analysis, and modeling; and the University of California at Berkeley conducts and administers research on economic analyses and policy issues. The Center also supports the Global Climate Change Grant Program, which offers competitive solicitations for climate research.

The California Climate Change Center Report Series details ongoing Center-sponsored research. As interim project results, these reports receive minimal editing, and the information contained in these reports may change; authors should be contacted for the most recent project results. By providing ready access to this timely research, the Center seeks to inform the public and expand dissemination of climate change information; thereby leveraging collaborative efforts and increasing the benefits of this research to California's citizens, environment, and economy.

For more information on the PIER Program, please visit the Energy Commission's website www.energy.ca.gov/pier/ or contact the Energy Commission at (916) 654-5164.

Table of Contents

List of Figures

List of Tables

Abstract

Using statistical models, wildfire risks are described as a function of climatic variables such as temperature and precipitation, and of hydrologic variables simulated using temperature and precipitation. Wildfire risks for the GFDL and PCM models and the A2 and B1 emissions scenarios are compared for 2005-2034, 2035-2064 and 2070-2099 against a 1961-1990 reference period to examine climate change scenarios ranging from neutral to lower precipitation and higher temperatures in California and neighboring states. We consider changes in wildfire risks for the larger region, California and northern and southern California.

Outcomes for the GFDL model runs, which exhibit higher temperatures than the PCM model runs, diverged sharply for different kinds of fire regimes, with increased temperatures promoting greater large fire frequency in wetter, forested areas, via the effects of warmer temperatures on fuel flammability. At the same time, reduce moisture availability due to lower precipitation and higher temperatures led to reduced fire risks in some locations where fuel flammability may be less important than the availability of fine fuels.

Property damages due to wildfires were also modeled using the 2000 U.S. Census to describe the location and density of residential structures. Structure values were determined from Census property values and empirically derived ratios describing the fraction of property values ascribed to structures and the fraction of structures within a fire perimeter that are on average destroyed in a fire. Our analysis determined that the largest changes in property damages under the climate change scenarios occurred in wildland/urban interfaces proximate to major metropolitan areas in coastal southern California, the Bay Area, and in the Sierra foothills northeast of Sacramento.

1.0 Part 1: Fire Modeling

(Anthony Westerling)

We developed a logistic regression model with piece-wise polynomials to estimate the probabilities of fires that exceed an arbitrary threshold of 200 hectares (approximately 500 acres) occurring in any given month as functions of climatologic, hydrologic and topographic variables. This model was estimated using observed fire frequency, precipitation, and temperature, and simulated hydrologic variables as a baseline. We then used this model to investigate how large fire risks would change under four scenarios for future climate. These scenarios, corresponding to "business as usual" (A2) and "transition to a low greenhouse gas emissions" (B1) emissions scenarios in two global climate models (GFDL and PCM), represented on average warmer, drier futures.

Fuel-limited fire regimes like desert grass and shrub lands responded differently to climate scenarios considered here than did energy limited fire regimes like mountain forests. In the former, changes in precipitation and temperature that reduce moisture availability sometimes led to a reduction in fire risks in our model, while in the latter, temperature increases in particular led to increased fire risks. Our results indicate a considerable divergence between outcomes for southern and northern California in the most extreme (in terms of temperature and precipitation) scenarios.

1.1 Domain and Resolution

This analysis covers California, Nevada, and parts of neighboring states on a 1/8-degree grid contained within 124.5625 to 113.0625 degrees West Longitude and 31.9375 to 43.9375 North Latitude. Fire histories and climatologic and hydrologic explanatory variables were aggregated to a monthly temporal resolution from 1980 to 1999. This yielded 93x97x240= 2165040 voxels (93 eighth-degrees of Latitude by 97 eighth-degrees of Longitude by 240 months).

The Pacific Ocean, some areas converted to agriculture or other uses, and grid cells corresponding to lands managed by agencies for which we had no fire histories (Department of Defense, Bureau of Reclamation, Fisheries and Wildlife Service, and the Department of Energy's Nevada Test Site) were masked out. An additional 240 voxels were excluded because we had no hydrologic data for them. The result was a 1490160-voxel domain covering California and contiguous parts of neighboring states by month from 1980-1999.

1.2 Data: Fire History

Fire occurrence data for fires greater than 200 hectares for 1980-1999 were compiled from the USDA Forest Service, from USDI's Bureau of Land Management, National Park Service, and Bureau of Indian Affairs, from the state lands or forestry agencies of Oregon, Utah, Arizona, and California, and from contract counties in California.

There were 3137 voxels (grid cell x month) where at least one fire exceeded 200 hectares in the sampled period, and 1487023 where no fires were observed above this minimum threshold. (See Figure 1 for the spatial extent of the fire record)

1.3 Data: Predictors

Precipitation, maximum temperature, VIC soil moistures and snow water equivalent, and elevation were examined as potential predictors for large fire risk.

For each voxel, a record was created containing the following variables:

SMI	soil moisture index from the VIC hydrologic model, estimating soil moisture as percent of total soil porosity.
SMI12m	maximum SMI over the preceding twelve months
SMI20	the average monthly SMI over the preceding twenty years.
WET	True/False factor: SMI20 >= 28%.
PREC	precipitation for the current month
PREC12	cumulative precipitation for the preceding twelve months
PREC12.6	PREC12 leading by six months
TMAX	monthly mean of daily maximum temperatures for the current month.
TAVG	mean March through August temperature for the current year
SI	snow index = 1 – SFI/12, where SFI is the average number of snow-free months over the preceding twenty years. It is the percent of the year a location has snow cover. Derived from VIC Snow Water Equivalent.
ELEV	mean elevation derived from GTOPO30 Global 30 Arc Second (~1km) Elevation Data Set, distributed by the North American Land Data Assimilation System (http://ldas.gsfc.nasa.gov/)

Monthly precipitation and maximum temperature concurrent with the fire month were selected as indicators of conditions for the ignition and spread of fire. Maximum soil moisture and cumulative precipitation over the preceding year(s) were selected as indicators of the moisture available for the production of fine fuels that can facilitate ignition and spread in subsequent fire seasons. Westerling et al. (2003) demonstrated the importance of a soil moisture proxy (i.e., the Palmer Drought Index) derived from temperature and precipitation for concurrent and subsequent wildfire activity on a regional basis for the western United States, and Westerling et al. (2001, 2002, 2003, 2004) and Preisler and Westerling (2005) have used similar variables to forecast wildfire activity on interannual to seasonal and monthly timescales.

Average spring and summer temperature was selected as an indicator of the timing of spring and thus the length of the dry season and, especially for higher elevation forests, the length and severity of the fire season (Westerling et al. 2005). Westerling et al. (2005) found the percentage of the year with snow cover is an important control on the effects of changes in the timing of spring on the length and severity of the fire season in mountain forests. Consequently, we use the interaction between these two variables (TAVG and SI) as a predictor for fire risks. It is important to note that monthly soil moisture alone does not capture the effect of a change in the timing of spring on fire

risks. An early spring results in an earlier arrival of summer drought, but may not lead to large changes in soil moisture for peak summer months, when these may be typically dry anyway, while the longer dry season is associated with greater fire risks in the peak summer months of the fire season.

Long-term average soil moisture and elevation are useful indicators of the nature of the local water balance, characterizing coarse vegetation types and the likelihood that soils and fuels will dry out regularly during the summer fire season. Notice in particular the strong correspondence between coarse vegetation types and available moisture (as described by long term average precipitation and soil moisture in Figure 1), and between available moisture and the incidence of large fires (grid cells with one or more large fires in the historical record are indicated in Figure 1).

The factor WET was used to categorize voxels in one of two fire regimes: a wet (or energy limited) fire regime and a dry (or fuel-limited) fire regime. This serves both to coarsely characterize vegetation type and the response of wildfire risks in that vegetation to climate.

1.4 Data: Simulation

The same hydrologic and climatologic variables as described above, were derived from GFDL and PCM global climate model runs for the A2 and B1 emissions scenarios. The downscaling and bias correction of the GCM precipitation and temperature follow statistical techniques originally developed by Wood et al. (2002, 2004), as described in the Scenarios Chapter (Cayan et al., this study). The downscaling and bias-correction methodology does not preserve the day-to-day variability from the GCM runs, with the result that changes in extremes may not be well represented.

The VIC hydrologic model (Liang et al. 1994, 1996) was run at 1/8-degree resolution over the entire domain using downscaled, bias corrected precipitation and temperature (Scenarios Chapter, Cayan et al, this study). An historical VIC run was also generated using temperature and precipitation from the gridded National Climatic Center Cooperative Observer station data set (Maurer et al. 2002). The VIC model used here was calibrated to match streamflow records at several points in California and the Northwest. While the streamflow records provide an integrative measure of hydrologic processes in the major drainage basins of the region, the resulting soil moistures were not independently validated against in situ measurements. Soil moistures from un-calibrated VIC runs appear to be more strongly associated with fire risks than were the calibrated soil moistures analyzed here.

The A2 high emissions scenario corresponds to a CO_2 concentration by end of century of more than three times the pre-industrial level, while the B1 low-emissions scenario results in a doubling of pre-industrial CO_2. The GFDL A2 model run had the greatest increase in temperature (> 4°C) and was the driest of the four scenarios used here. This scenario was at the high end of temperature changes over California compared to an ensemble of IPCC AR4 model simulations (Cayan et al. this study). The PCM B1 scenario had the lowest temperature increase and little or no change in precipitation. The GFDL B1 and PCM A2 runs represented neutral (PCM A2) to moderately dry (GFDL B1) scenarios with intermediate temperature increases (<°3 C) over California,

placing them close to the average scenario from an ensemble of IPCC AR4 model simulations (Cayan et al. this study).

1.5 Methodology

Adopting the forecast methodology used in Preisler et al. (2004) and Preisler and Westerling (2005), we estimate the probability of at least one large fire occurring in a voxel via a logistic regression. Our predictand is the probability that a fire exceeds an arbitrary size threshold:

$$P_{i,j,t} = \text{Prob}[A_{i,j,t} > C \mid X_{i,j,t}, e]$$

where $P_{i,j,t}$ is the probability that the voxel denoted by longitude = i, latitude = j, time = t contains at least one fire greater than C (where C = 200 hectares) given a vector of predictor variables $X_{i,j,t}$. In this case $X_{i,j,t}$ denotes the record of predictor variables introduced in the previous section for the voxel indexed by i, j, and t.

Because the relationships between P and several of the predictor variables are nonlinear, a nonlinear model using basis splines was estimated using the R statistical package (R Development Core Team 2004). The bs() function in R was used to create basis functions for TMAX, PREC12, PREC12.6, and ELEV. The boundary knots for the PREC12, PREC12.6 and TMAX basis splines were set to limits greater than the range of variability in the climate simulations. A thin plate spline (Hastie et al. 2001, Preisler et al. 2004, Preisler and Westerling 2005) was used to estimate a two-dimensional surface describing the interaction between SI and TAVG, with the boundary knots for TAVG also set to limits greater than the range of variability in the climate simulations.

The glm() function in R was used in conjunction with smartpred library developed by Thomas Yee (http://www.stat.auckland.ac.nz/~yee/smartpred/index.shtml) implementing an algorithm devised by Chambers and Hastie (1992) to fit a generalized linear model (Dobson 1990) and to make predictions using that model on simulated climatologic and hydrologic variables.

The model specification is:

$$\text{Logit}(P) = A_{WET} + B_{WET} \times [X(\text{TMAX}) + X(\text{PREC12}) + X(\text{PREC12.6}) + X(\text{ELEV}) + X(\text{SI,TAVG}) + \text{PREC} + \text{SMI12m} + \text{SMI20}]$$

Where $X(V_i)_{wet}$ is a matrix describing a basis spline for V = { TMAX, PREC12, PREC12.6, ELEV, SI*TAVG } and WET = {TRUE, FALSE}, and A and B are parameter vectors estimated from the data.

This specification is motivated by recent work (e.g., Swetnam and Betancourt 1998, Kipfmueller and Swetnam 2000, Veblen et al. 2000, Donnegan et al. 2001, Heyerdahl, Brubaker and Agee 2002, Westerling et al. 2003 and 2005) describing associations between fire activity and antecedent and concurrent climate conditions. In particular, the work of Westerling and of Preisler (D.R. Brillinger et al. 2003, Preisler et al. 2004, Preisler and Westerling et al. 2005) in describing statistical forecast and modeling methodologies for western U.S. wildfire guide this work.

As a crude simplification, this model specification assumes two fire regimes: a wet, or energy-limited, regime and a dry, or fuel-limited regime. All of the predictors are highly significant for both the wet and dry specifications, but the dry model is particularly sensitive to antecedent moisture as captured by SMI12m, PREC12 and PREC12.6, while the wet model puts greater weight on TMAX and interactions between TAVG and SI. This difference is consistent with some common hypotheses regarding climate – fuel interactions. First, that dry western grass and shrublands have fuel-limited fire regimes, and thus are sensitive to antecedent moisture anomalies that promote the growth of fine fuels (Westerling et al. 2002, 2003). Second, that since the West's forests are relatively mesic they have abundant fuels, and thus their fire risks are limited less by fine fuel availability than by the energy available to dry live vegetation and dead fuels during the summer fire season (Swetnam and Betancourt 1998). SI is an indicator of the length of the summer fire season, and of the importance of spring and summer temperature anomalies in extending the dry, snow-free season (Westerling 2005).

Vegetation type is an important factor for characterizing both fire dynamics and hydrology. For the latter, we were constrained to use the VIC hydrologic model with a fixed vegetation layer that did not evolve with a changing climate. In the statistical fire model specification, we use average soil moisture and snow water equivalent over the preceding 20 years for each voxel to characterize the fire regime response to temperature and to antecedent moisture. These parameters are relatively static during the reference period (1961-1990), but have the potential to vary freely as the climate simulation unfolds. Because these data are only available starting in 1950, SI and WET were fixed for the first ten years of the reference period to the values derived from the 1950–1969 averages for SWE and SMI.

The estimated logistic model fits the observed data aggregated along multiple dimensions. Since the model response is a probability, it is necessary to aggregate the data in some way to facilitate comparisons with the observed data. Binning the observed large fire incidence by increments of 0.1 in the linear predictor for the logit, we see a tight fit between the estimated logit and the observations (Figure 2). Despite the lack of a dummy variable for month, the seasonal cycle in the estimates approximates the observed cycle (solid and dashed black lines in Figure 3). This result is driven purely by the cyclicality in the observed climate and simulated hydrologic data.

The interannual variability in the observed data is also captured reasonably well by the model, with the correlation between the two at 0.78 (Figure 4). Finally, the spatial pattern of estimated fire risk (Figure 5) is a good approximation of the spatial pattern in the observed fire risk. Given that the model specification is limited to climatic variables and elevation, the latter of which does not vary over time, it is clear that climate plays an important role in driving variability in wildfire.

1.6 Results

A2 scenarios exhibited a greater increase in large fire risk than B1 scenarios, and GFDL a greater increase than PCM models, by mid-century (Figures 6 and 7). Increases by 2070-2099 ranged from just over 10% to just under 40% increases over-all in large fire risk over the whole region. For California only, changes by the end of the century ranged

from an increase of 12% to 53% (Table 1). Within California, increases in Northern California ranged from 15% to 90%, while Southern California ranged from a decrease of 29% to an increase of 28% (Table 1, Figures 8–10 and 11–14). Unlike the results for either Northern California or the region as a whole, both GFDL model runs showed decreases in fire activity for Southern California by the end of the century.

While the higher temperatures in the GFDL model runs tended to promote fire risk overall, reductions in moisture due to lower precipitation and higher temperatures led to reduced fire risk in dry areas that appear to have fuel-limited, and thus moisture-limited fire regimes. The effects of lower moisture availability on fine fuel production outweighed the effects of temperature on fuel flammability in dry grass and shrub lands at lower elevations. This effect was particularly pronounced in much of southern California and western Arizona (Figure 8–10). By contrast, the effects of temperature and lower precipitation in the GFDL runs produced larger increases in the western slopes and foothills of the Sierra Nevada and in the Coast and Cascade ranges of northern California and southern Oregon, where forests and woodlands provide a ready source of fuel.

These model results indicate that scenarios that tend toward hot and dry extremes will tend to produce opposite results in fuel-limited versus energy-limited fire regimes, with decreased fire risk over time in the former and increased risk in the latter. Conversely, wetter scenarios with more moderate temperature increases may actually result in more fire overall, as in A2 PCM versus B1 GFDL in this instance, (Table 1). The combination of models and scenarios compared in this analysis all had warmer temperatures and neutral to reduced precipitation. It would be interesting to see if a warmer, wetter scenario produces significantly more fire than did these warmer, drier scenarios.

It is important to keep in mind the highly variable nature of fire risks from year to year (see Figure 6). Scenarios with elevated fire risks on average can still produce years with very little fire, and vice versa.

Santa Ana winds are an important component of wildfire risks in southern California that are not modeled here. To the extent that climate change could affect the frequency, strength, and/or duration of Santa Ana wind events, the results for southern California could be affected. Preliminary results of a Santa Ana wind analysis (Miller and Schligell, this study) indicate, however, that the frequency of Santa Ana events may decrease by the end of the century, which would serve to reinforce any reductions in southern California fire risks due to changes in temperature and precipitation.

2.0 Part 2: Loss Modeling

(Anthony Westerling, Benjamin Bryant)

To estimate the economic damage caused by wildfires, we developed a program that works by associating spatial property data with the geographic location of past and hypothetical wildfires. For this report, we estimated the expected number of structures at risk, structures lost, and the value of these structures, for wildfires 200 hectares in size in California. Since our logistic probability model estimated the risk of fires equal to or greater than 200 hectares in size, the damages reported here are our best currently available estimate of the expected minimum impact of wildfire for the four climate change scenarios considered here on property. It is important to keep in mind as well that these damages represent just one dimension of the economic impact of wildfire. Fire suppression and prevention expenditures, health effects of fire-caused pollution, effects on subsequent runoff, flooding, erosion and water quality, altered recreation opportunities, loss of forest and range resources, habitat changes, and altered passive uses (e.g., views) all have their own costs and benefits that reflect economic impacts of wildfire.

2.1 Data and Methodology

We first created a finely spaced grid of over half a million points covering California, and then associated each point with the US census block group in which it lies. According the Census Bureau, "a block group is the smallest geographic unit for which the Census Bureau tabulates sample data [including housing and property value data]. Block groups vary in area but encompass on average about 1500 people. There are 22133 contained within California. (http://factfinder.census.gov). Given any set of points (selected either randomly or from historical fire perimeters), we can use the census data and derived values to estimate total quantities of interest (e.g., number of structures, total property value) contained within the area associated with those gridpoints. Lastly, to estimate damage caused by fires, we multiply the values contained within the area by empirically derived ratios for improved structure value and the number of structures destroyed given that a fire perimeter encompassed the structures.

Linking of geographic and census data was accomplished using the R statistical programming language. We created functions to extract relevant census data from "Summary File 3" for California, which is available free from the Census Bureau website. This provided information including population, number and distribution of housing units, and property value estimations for owner-occupied housing units. We required an estimate of both total housing structures, as well as total property value within a census block. These we derived by developing weighting and scaling functions that utilize block-group-specific information on how many housing units are in structures of various sizes, combined with how many housing units were occupied by the owner, versus those that were rented or vacant.

Next, we utilized the Census Bureau's census block cartographic boundary files to associate the demographic data with our finely spaced grid covering California. The boundary files provide data on the geography of each block group, thus allowing us to identify which block group each point in our grid falls into. The quantities associated

with that block group are then associated with the gridpoint, except scaled down according to the area fraction of the block group represented by the grid point. Given a region which encompasses a set of grid points, we simply sum the values associated with those gridpoints to get an estimate of the quantities contained within that region.

Note that this assumes a homogeneity within block groups. However, the heterogeneity that exists should be effectively random, so that given the number of samplings used in this report, the effect is expected to be minimal. The homogeneity assumption may break down in extremely large block groups, but very large block groups occur when housing is very sparse, and since values are scaled down by area, the error contributed to the aggregate damage estimates should again be minimal. In general, the results should be interpreted statistically, not on a case by case basis.

Lastly, to estimate damages, we require a method for scaling total value enclosed to total value damaged. This is controlled by two factors: The fraction of structures damaged given they were encompassed by a fire perimeter, and the fraction of a property's value associated with improvements to the property (which is the fraction assumed to be lost if the home is burned). For the latter, we use estimates provided by the California Department of Forestry and Fire Protection's Fire and Resource Assessment Program (FRAP) derived from county assessors parcel data for Mariposa and Nevada counties (Robin Marose, personal communication).

To estimate the damage ratio as a function of structure density, we extracted data from archived Incident Management Situation Reports ("SIT reports") of past large fires in California (http://iys.cidi.org/wildfire/). These reports provided an estimate of the number of structures destroyed in each fire. We then used GIS information about the fires boundaries to identify points on our grid contained within the fires, and used those to estimate the total number of structures contained within the fire perimeter. We then used the information combining structures contained, structures damaged and area to generate a linear model approximating the expected value for the damage ratio, given a structure density. Note that we assume that structures termed as "lost" in the SIT reports were a total loss: we do not try to estimate the percent of a structure that is lost.

Because of the lengthy string of steps involved in creating it, the accuracy and meaningfulness of the damage ratio is likely the least certain link in the chain from data to fire estimates. In particular, the linking of fire-perimeters data with structures-damaged data was subject to significant uncertainty due to a lack of common and unambiguous identifying information. Matching was performed only by character matching of the fire names, which were not standardized, in combination with dates. Fortunately, the effect of the damage ratio on damage estimates is effectively linear, so it is easy to note how the estimates will change given an error in the damage ratio function.

The results of this analysis should not be particularly sensitive to either the damage ratio or the improved ratio selected. The greatest increases and decreases in value for burned structures under the climate change scenarios were found to occur in gridcells that are very similar in terms of structure density and proximity to urban areas. Consequently, we expect them to have similar improved ratios and damage ratios. While the choice of

ratios would affect the level of estimated damages in these gridpoints, given the similarity of the locations, it would not be expected to have a large affect on the change in damages under a climate change scenario relative to the reference period. This is in part due to the fact that we hold development fixed at the 2000 census. If we were to complicate this analysis by projecting future development scenarios, then the choice of improved and damage ratios might have a greater impact on the change in damages. This would be especially true for scenarios that posited more development in higher elevation forests that are presently sparsely populated but which account for much of the increased fire risk under the climate change scenarios considered here.

To generate the values used in this report, we approximated the effect of a 200 hectare fire in each of 2440 1/8 degree cells covering California. A 200-hectare fire is represented in most cases by 2 gridpoints, so for each 1/8 degree cell we randomly chose two points and aggregated their values, applying the formulas described above, with some appropriate scaling to account for the discrete nature of the gridpoints. We repeat this process 100 times for each gridcell, and then retain the mean value for the number of structures at risk (i.e., contained within fire perimeters), the number of structures burned, and the value of the burned structures. To estimate the expectation for each of these values under each climate scenario, we multiply them by the estimated probability of a large fire in each corresponding voxel from Part 1 above.

2.2 Results

The total expected values estimated for structures burned in this analysis were dominated by changes in wildfire risks proximate to a few urban areas with an extensive wildland urban interface: basically coastal counties of southern California, areas adjacent to the Bay Area, and northeast of Sacramento along Interstate Highway 80 (Figure 15). While fire risks increase dramatically in the GFDL A2 scenario in the Sierras and Coast and Cascade ranges of northern California, for example, most of these areas are relatively sparsely populated, with relatively few structures based on the 2000 census in harms way compared to the environs of the coastal cities. Similarly, increases or reductions in fire risks over much of the inland deserts of southern California appear to have a similarly muted effect.

Comparing Northern to Southern California based on the distribution of residential property in the 2000 census, the value of burned property in northern California nearly doubles (+96%) in the GFDL A2 scenario, accounting for all of the statewide increase in property damages in that scenario. Likewise, in the scenario with the least pronounced temperature increase (PCM B1), increased damages in Northern California account for all the increase in California (Table 1).

Perhaps the most interesting result of this analysis is the effect of substantial increases in fire risks in the Sierra foothills in the GFDL A2 scenario on property damages northeast of Sacramento, a county whose population has been growing at about a 2.3% per year rate in the last five years. GFDL A2 is admittedly the most extreme scenario considered here, but it is instructive in that it draws attention to developing vulnerabilities in a rapidly-growing part of the state. A lesser increase in temperature and fire risk may still exacerbate vulnerabilities that may develop around future development.

The key policy consideration for climate change impacts for wildfire in California is going to revolve around scenarios for future development. As California's population grows in the coming decades, decisions on where to locate future development will shape California's vulnerability to any climate change-induced increases in wildfire risks. In particular, development that expands the wildland/urban interface in the foothills and mountains of northern California would, based on this analysis, appear to increase vulnerability to property losses due to wildfire.

3.0 References

Balling, R. C., G. A. Meyer, and S. G. Wells, 1992: Relation of Surface Climate and Burned Area in Yellowstone National Park. *Agric. For. Meteor.*, **60**, 285-293.

D.R. Brillinger, H.K. Preisler, and J.W. Benoit. 2003. "Risk assessment: a forest fire example." In Science and Statistics, Institute of Mathematical Statistics Lecture Notes. Monograph Series.

Chambers, J. M. and Hastie, T. J. (eds.) (1992) Statistical Models in S. Wadsworth and Brooks/Cole, Pacific Grove, CA.

Dobson, A. J. (1990) *An Introduction to Generalized Linear Models.* London: Chapman and Hall.

Donnegan JA, Veblen TT, Sibold SS (2001) Climatic and human influences on fire history in Pike National Forest, central Colorado. Canadian Journal of Forest Research, 31, 1527-1539.

Friedman, J. H. (1984) SMART User's Guide. Laboratory for Computational Statistics, Stanford University Technical Report No. 1.

Friedman, J. H. (1984) A variable span scatterplot smoother. Laboratory for Computational Statistics, Stanford University Technical Report No. 5.

Hastie, T.J., Tibshirani, R., Friedman, J. 2001. *The Elements of Statistical Learning*. Data Mining, Inference, and Prediction. Springer, New York. 533 pp.

Heyerdahl, E.K, L.B. Brubaker, and J.K. Agee. 2001. Factors controlling spatial variation in historical fire regimes: A multiscale example from the interior West, USA. Ecology 82(3): 660-678.

Kipfmueller KF, Swetnam TW (2000) Fire-Climate Interactions in the Selway-Bitterroot Wilderness Area. USDA Forest Service Proceedings RMRS-P-15-vol-5.

Liang, X., D. P. Lettenmaier, E. Wood, and S. J. Burges (1994), A simple hydrologically based model of land surface water and energy fluxes for general circulation models, *Journal of Geophysical Research*, *99*, 14,415-414,428.

Liang, X., D. P. Lettenmaier, and E. F. Wood (1996), One-dimensional statistical dynamic representation of subgrid spatial variability of precipitation in the two-layer variable infiltration capacity model, *Journal of Geophysical Research*, *101*, 21,403-421,422.

Maurer, E. P., Wood, A. W., Adam, J. C., Lettenmaier, D. P. & Nijssen, B. (2002) *J. Clim.* **15,** 3237–3251

Preisler, H.K., D.R. Brillinger, R.E. Burgan, and J.W. Benoit. 2004. "Probability based models for estimating wildfire risk". International Journal of Wildland Fire, 13, 133-142.

Preisler, H.K., and A.L. Westerling 2005: "Estimating Risk Probabilities for Wildland Fires," ***Proceedings of the 2005 Joint Statistical Meetings***, Minneapolis, MN.

R Development Core Team (2004). R: A language and environment for statistical computing. R Foundation for Statistical Computing, Vienna, Austria. ISBN 3-900051-07-0, URL http://www.R-project.org.

Swetnam, T. W. and J. L. Betancourt, 1998: Mesoscale Disturbance and Ecological Response to Decadal Climatic Variability in the American Southwest. *Journal of Climate*,**11**, 3128-3147.

Veblen TT, Kitzberger T, Donnegan J (2000) Climatic and human influences on fire regimes in ponderosa pine forests in the Colorado Front Range. Ecological Applications. 10, 1178-1195.

Westerling, A.L., A. Gershunov, D.R. Cayan and T.P. Barnett, 2002: "Long Lead Statistical Forecasts of Western U.S. Wildfire Area Burned," International Journal of Wildland Fire, 11(3,4) 257-266.

Westerling, A.L., T.J. Brown, A. Gershunov, D.R. Cayan and M.D. Dettinger, 2003: "Climate and Wildfire in the Western United States," Bulletin of the American Meteorological Society, 84(5) 595-604.

Westerling, A.L., A. Gershunov and D.R. Cayan, 2003: "Statistical Forecasts of the 2003 Western Wildfire Season Using Canonical Correlation Analysis," ***Experimental Long-Lead Forecast Bulletin***, 12(1,2).

Westerling, A.L. and Swethnam, T. W. 2003. Interannual to Decadal Drought and Wildfire in the Western United States. EOS, vol 84, 545-560.

Westerling, A. L., H. Hidalgo, D.R. Cayan, and T. Swetnam, 2005: Trends in large wildfires in western U.S. forests since 1970: Affects of changes in the timing of Spring. In preparation.

Wood, A. W., L. R. Leung, V. Sridhar, and D. P. Lettenmaier (2004), Hydrologic implications of dynamical and statistical approaches to downscaling climate model outputs, *Climatic Change*, *62*, 189-216.

Wood, A. W., E. P. Maurer, A. Kumar, and D. P. Lettenmaier (2002), Long-range experimental hydrologic forecasting for the eastern United States, *Journal of Geophysical Research-Atmospheres*, *107*, 4429.

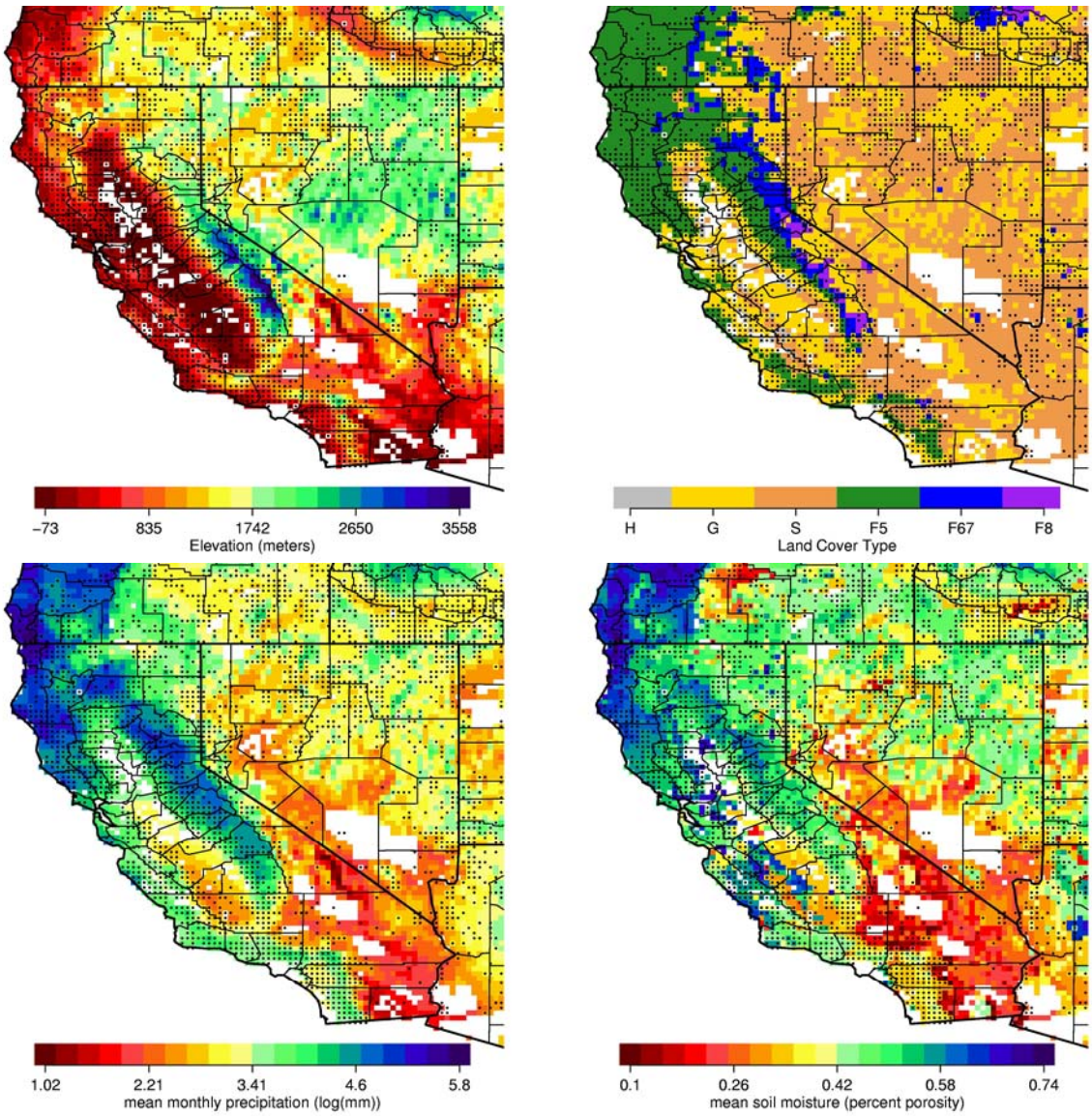

Figure 1. Top left: Elevation. Top right: Dominant vegetation type. Bottom left: Monthly mean precipitation 1970-1989. Bottom right: VIC modeled soil moisture. White areas are masked out (Pacific Ocean, urban and agricultural conversion, and land management agencies not included in our fire history). Black dots indicate a grid cell with at least one fire > 200 ha in our fire history. All variables plotted on a 1/8 degree grid.

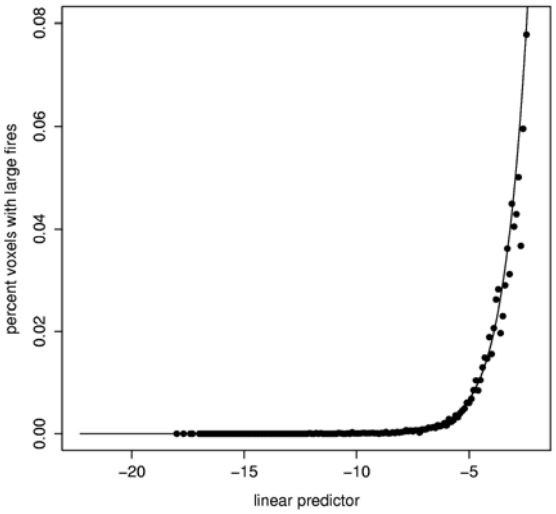

Figure 2. The estimated logit(P) (line), where P is the probability of observing a fire > 200 hectares in a voxel, versus the observed probabilities for 1980-1999 (points).

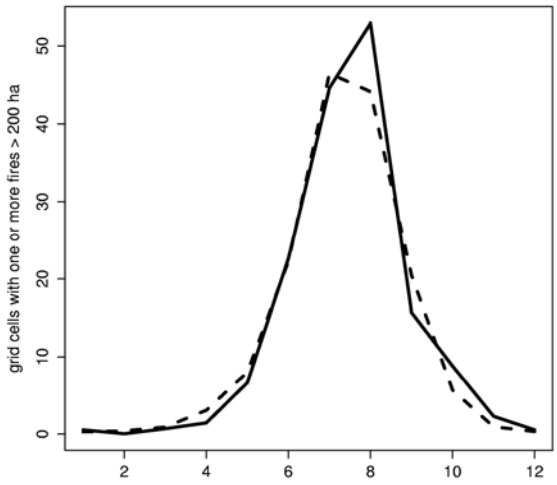

Figure 3. Comparison of seasonal cycles for the 1980-1999 model estimation period. Fitted values (dashed) versus observed (solid).

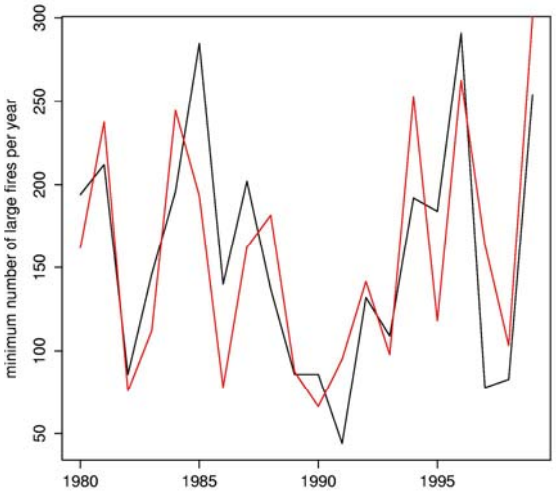

Figure 4. Expected voxels with fires > 200 hectares (dashed) estimated by logistic regression, by year, versus observed voxels with fires > 200 hectares (solid), by year, 1980–1999.

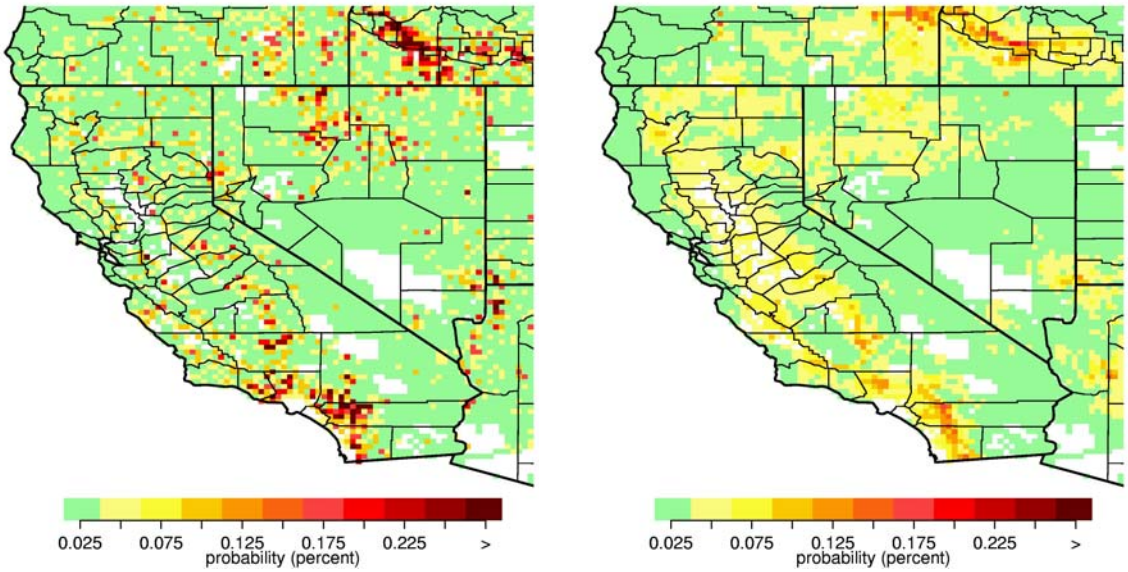

Figure 5. Observed (left) versus modeled (right) annualized risk of one or more fires > 200 hectares, 1981-1999. Observed risk, based on only 20 years' records, is necessarily more "noisy" than the logistic model.

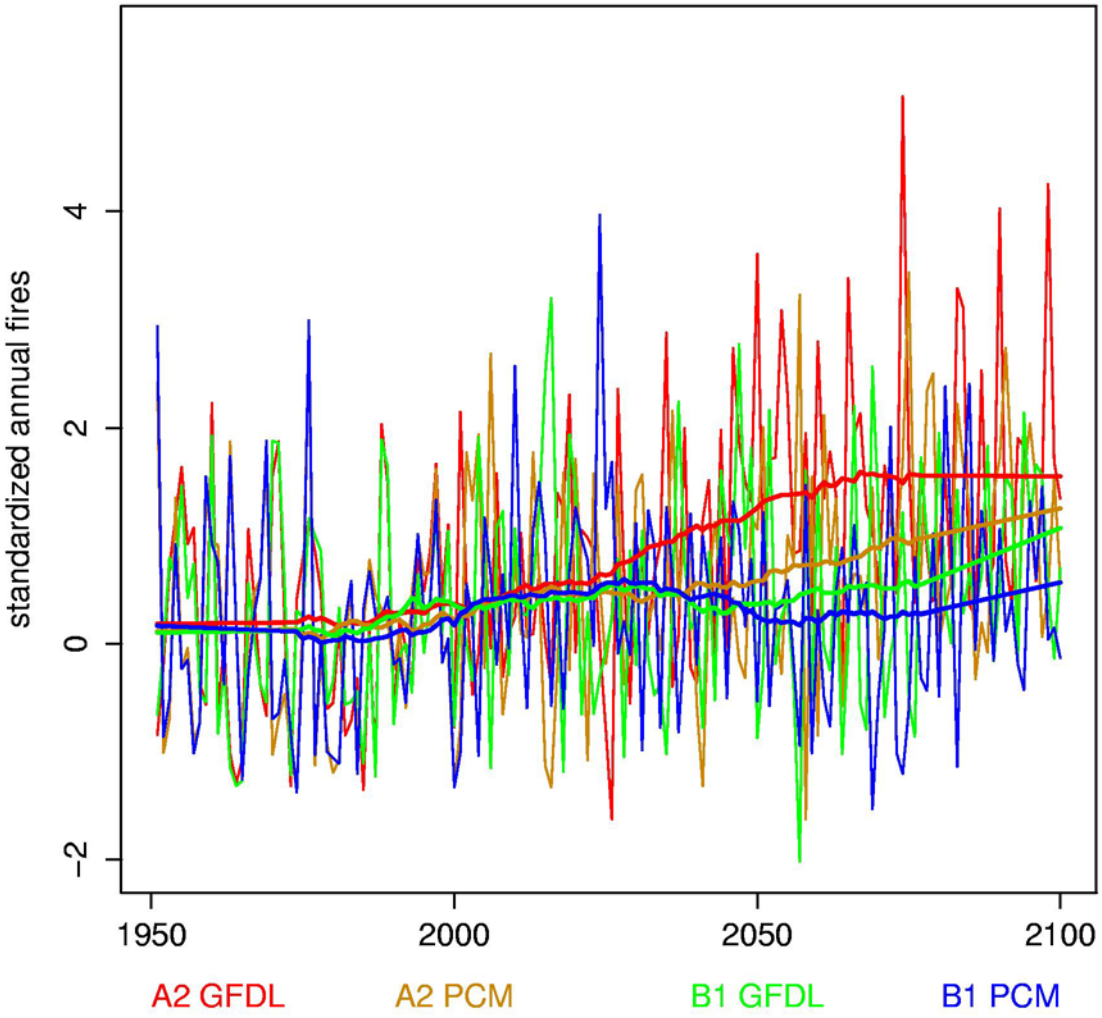

Figure 6. Standardized annual expected number of 1/8 degree x month voxels with at least one large fire (>200 ha) 1951 – 2100 for A2 and B1 emissions scenarios and GFDL and PCM global climate models. Bold lines are the result of smoothing with Friedman's supersmoother (Friedman 1984) with a span of 0.3.

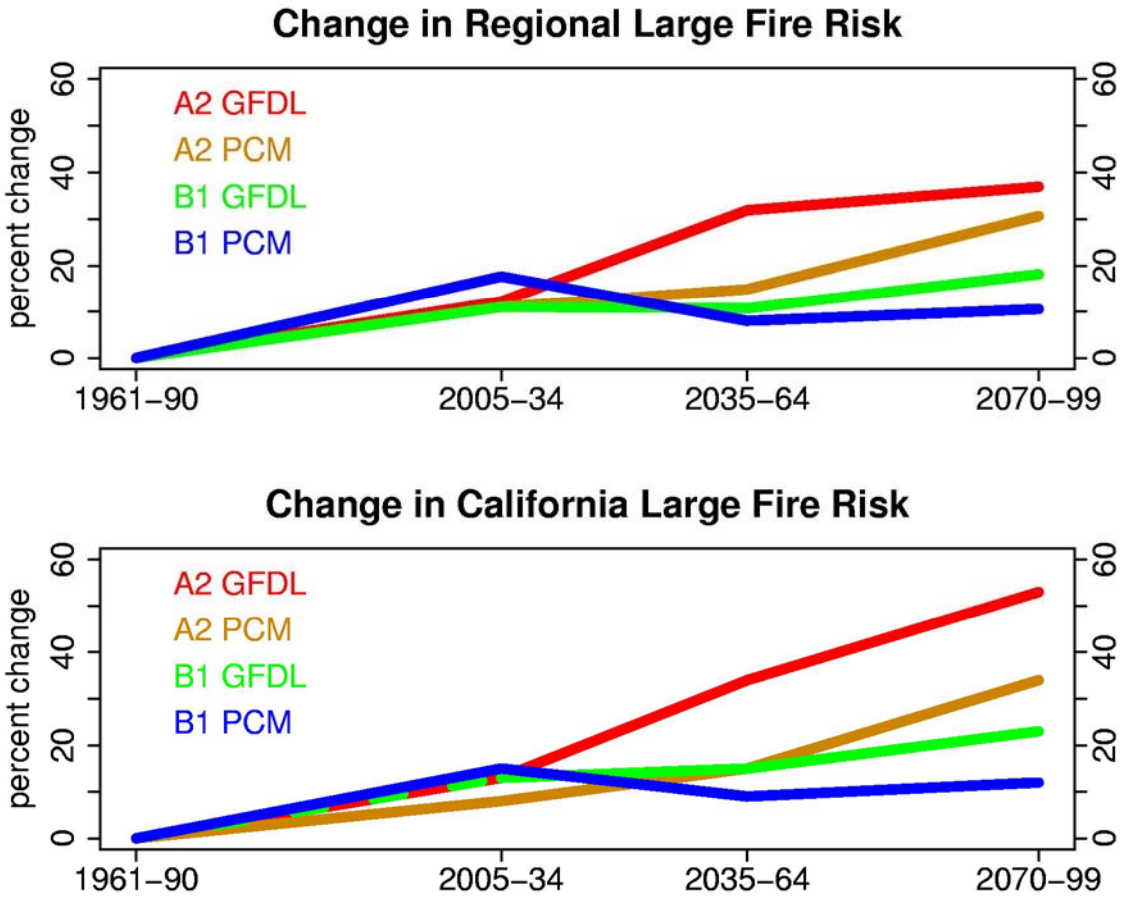

Figure 7. Percent change in the expected annual number of voxels (i.e., lat x lon x month) with at least one fire > 200 hectares for (*top*) region (California + neighboring states) and (*bottom*) California only.

A2 GFDL 2070-99 minus 1961-90

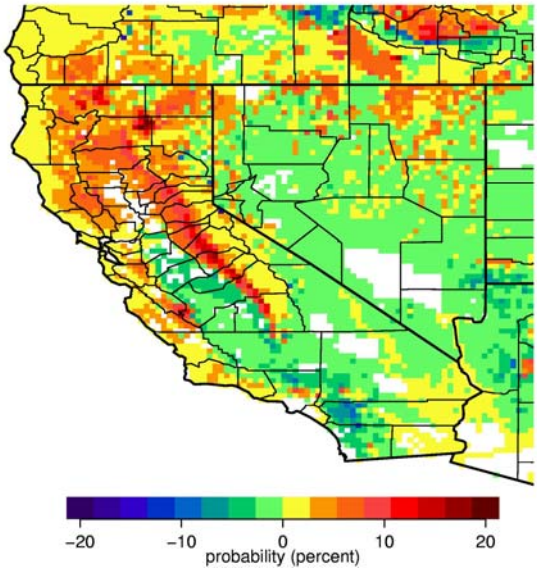

A2 PCM 2070-99 minus 1961-90

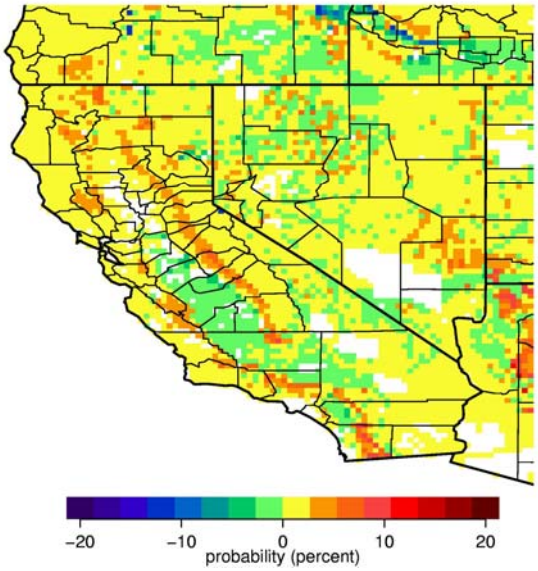

B1 GFDL 2070-99 minus 1961-90

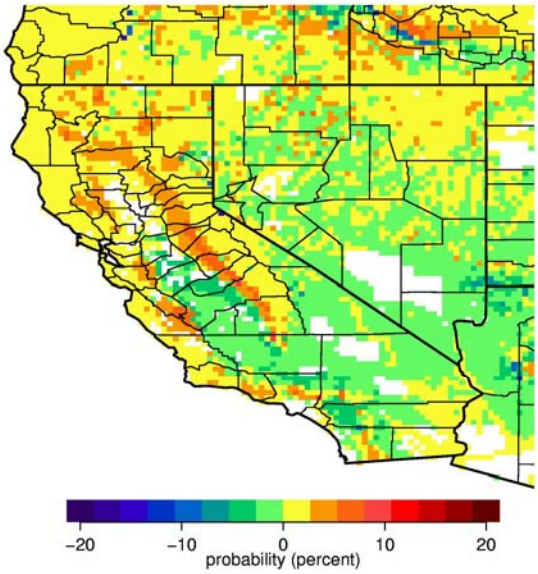

B1 PCM 2070-99 minus 1961-90

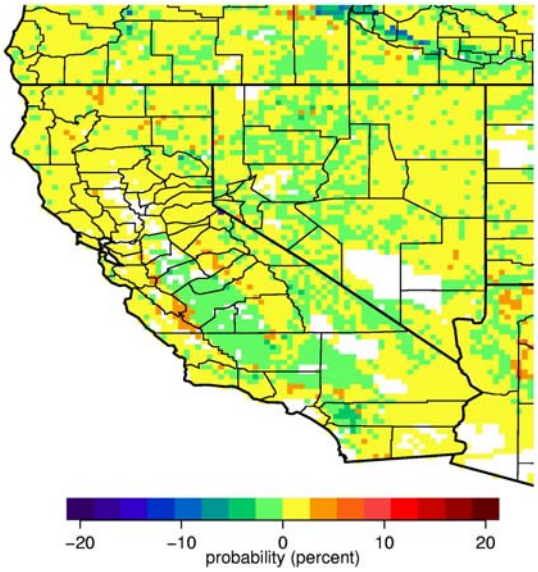

Figure 8. Difference (2070-2099 minus 1961-1990) in estimated average annual probabilities of at least one fire > 200 hectares for A2 and B1 emissions scenarios for GFDL and PCM models.

A2 GFDL 2035-64 minus 1961-90

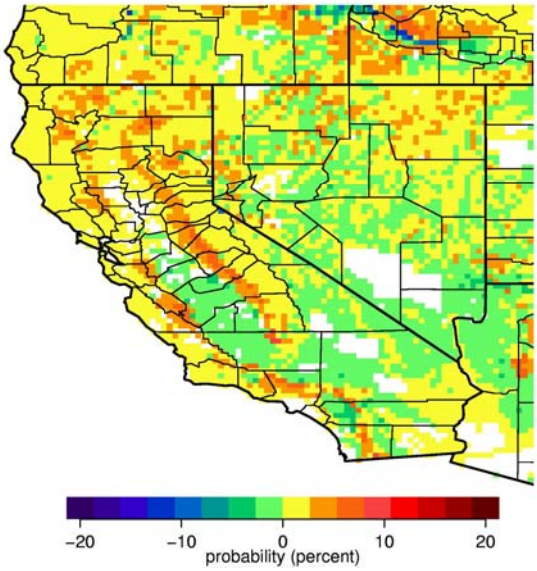

A2 PCM 2035-64 minus 1961-90

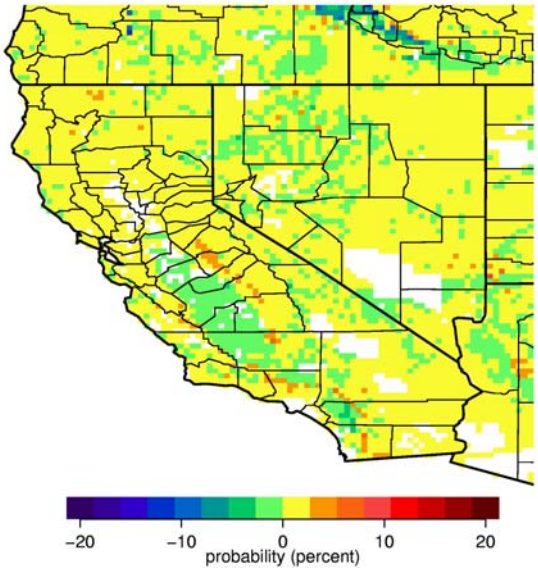

B1 GFDL 2035-64 minus 1961-90

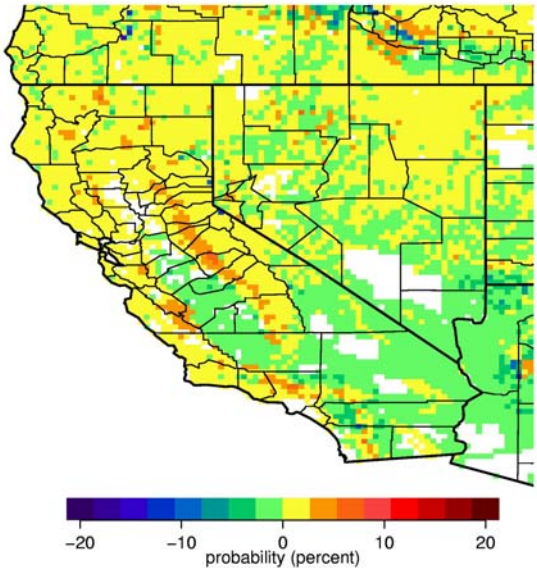

B1 PCM 2035-64 minus 1961-90

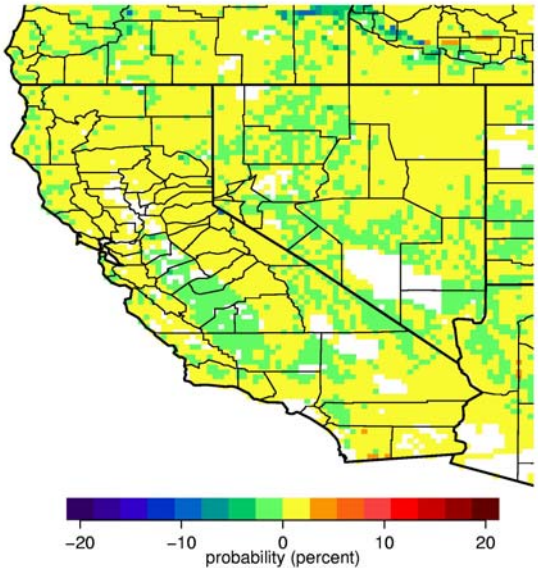

Figure 9. Difference (2035-2064 minus 1961-1990) in estimated average annual probabilities of at least one fire > 200 hectares for A2 and B1 emissions scenarios for GFDL and PCM models.

A2 GFDL 2005-34 minus 1961-90

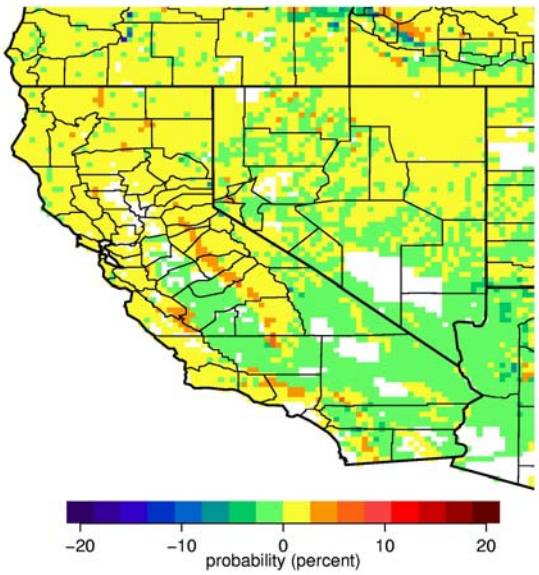

A2 PCM 2005-34 minus 1961-90

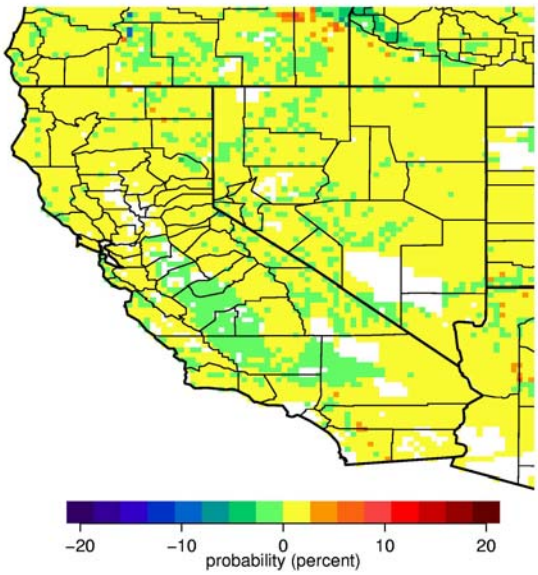

B1 GFDL 2005-34 minus 1961-90

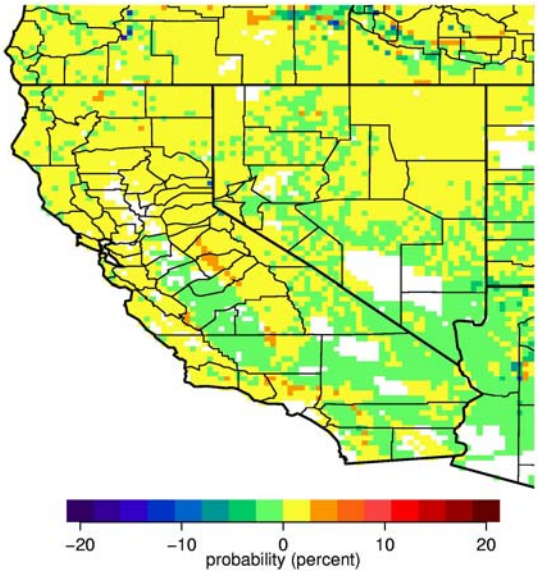

B1 PCM 2005-34 minus 1961-90

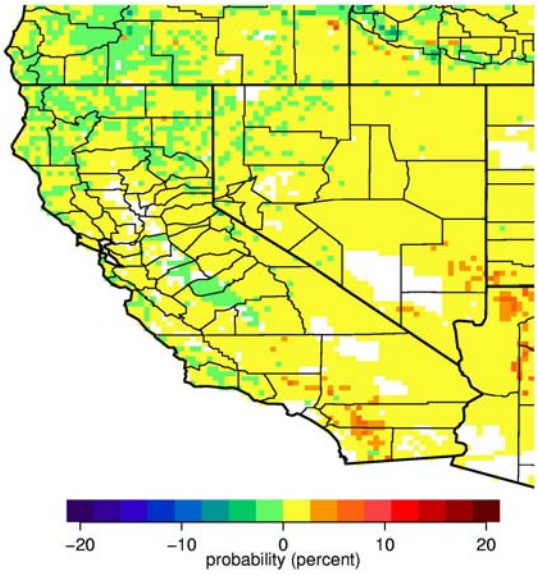

Figure 10. Difference (2005-2034 minus 1961-1990) in estimated average annual probabilities of at least one fire > 200 hectares for A2 and B1 emmisions scenarios for GFDL and PCM models.

A2 GFDL 1961-1990

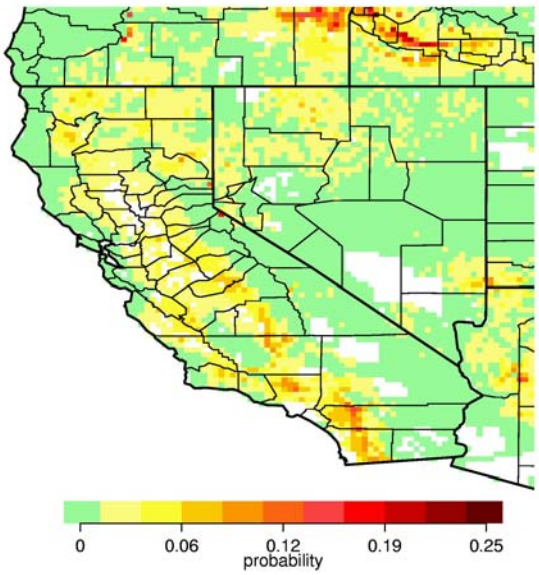

A2 GFDL 2005-2034

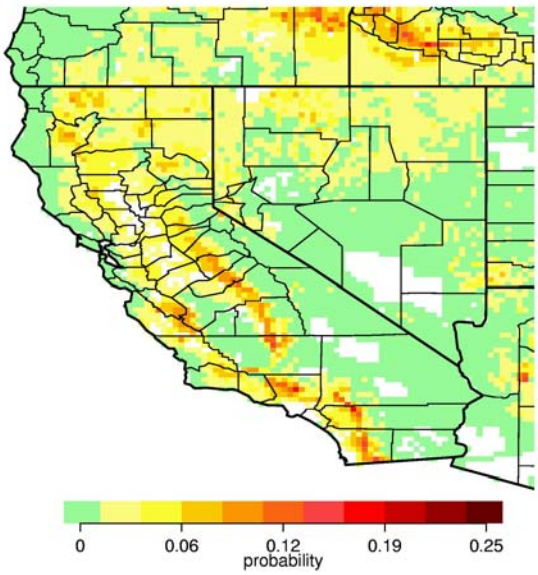

A2 GFDL 2035-2064

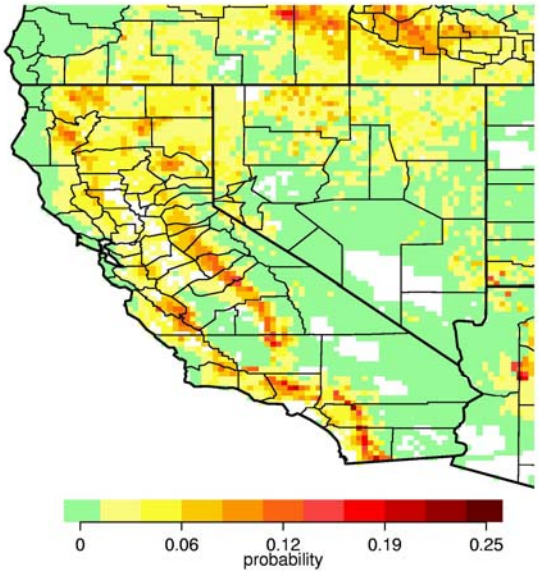

A2 GFDL 2070 - 2099

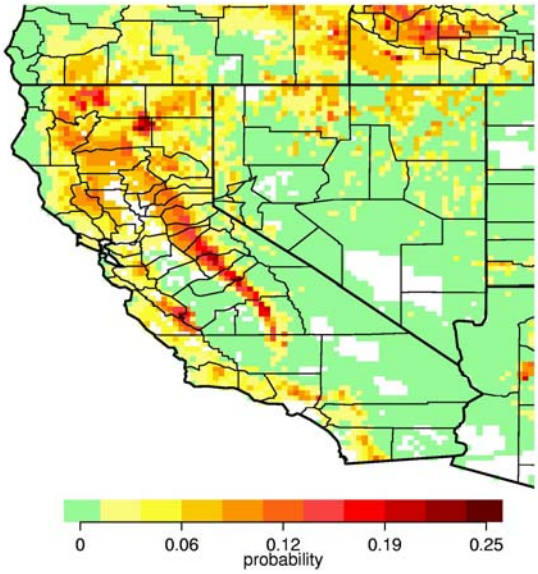

Figure 11. A2 GFDL estimated average annual probabilities of at least one fire > 200 hectares for 1961-1990, 2005-2034, 2035-2064, 2070-2099.

A2 PCM 1961-1990

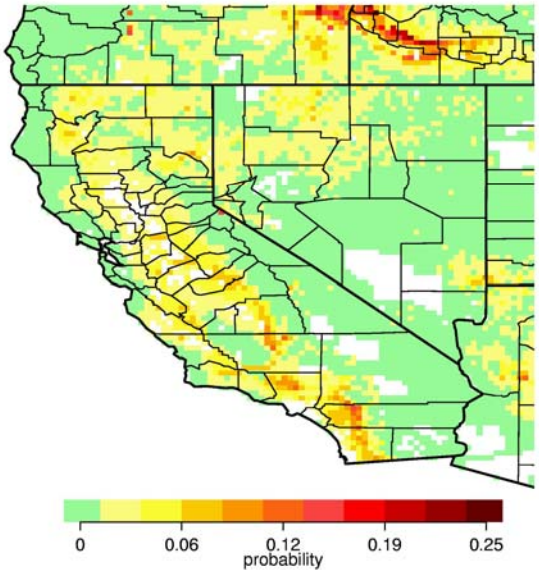

A2 PCM 2005-2034

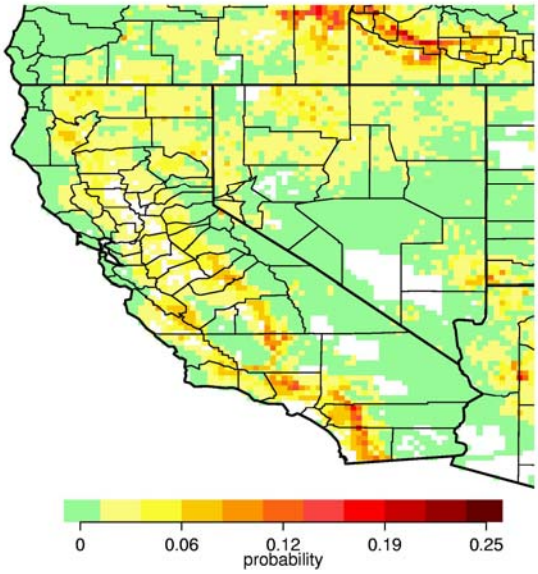

A2 PCM 2035-2064

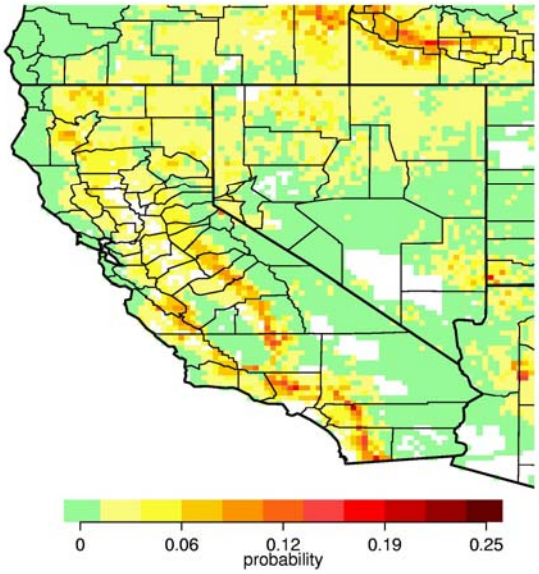

A2 PCM 2070 - 2099

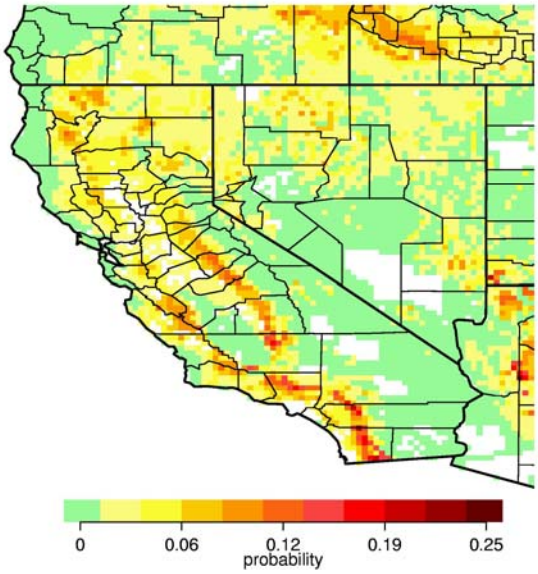

Figure 12. A2 PCM estimated average annual probabilities of at least one fire > 200 hectares for 1961-1990, 2005-2034, 2035-2064, 2070-2099.

B1 GFDL 1961-1990

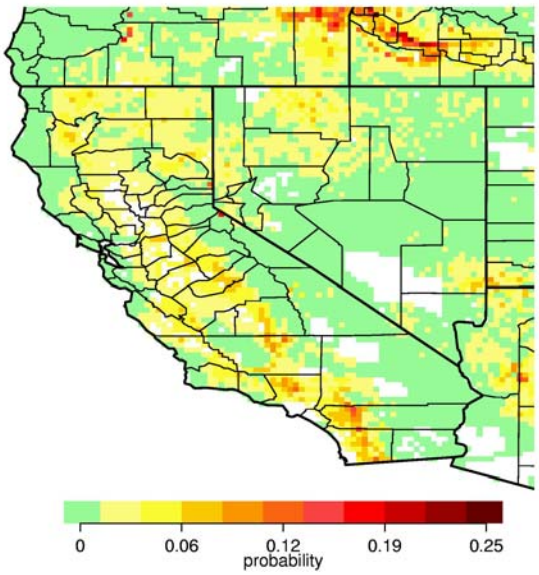

B1 GFDL 2005-2034

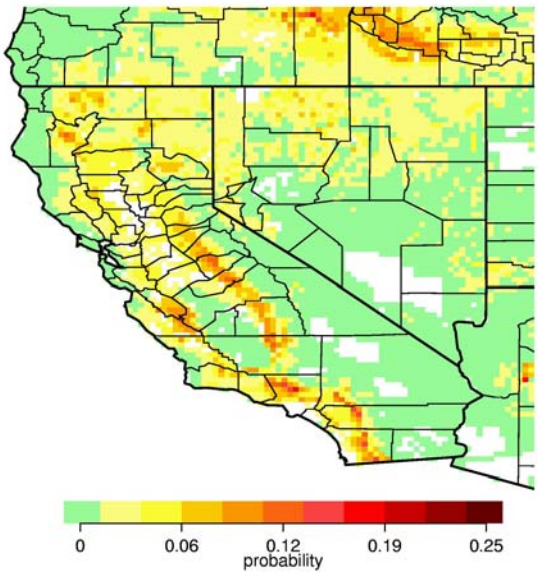

B1 GFDL 2035-2064

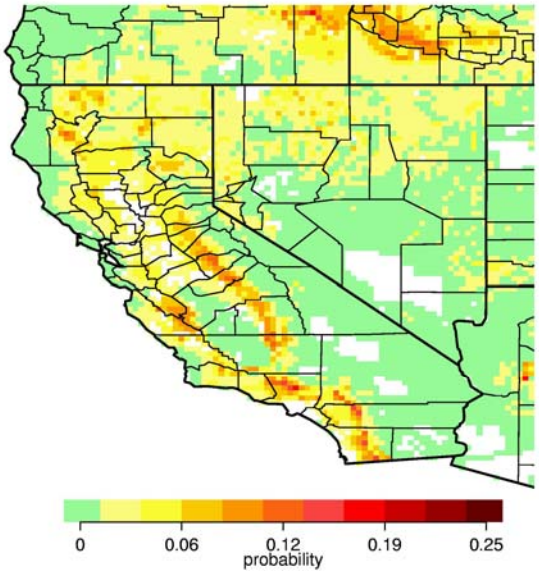

B1 GFDL 2070 - 2099

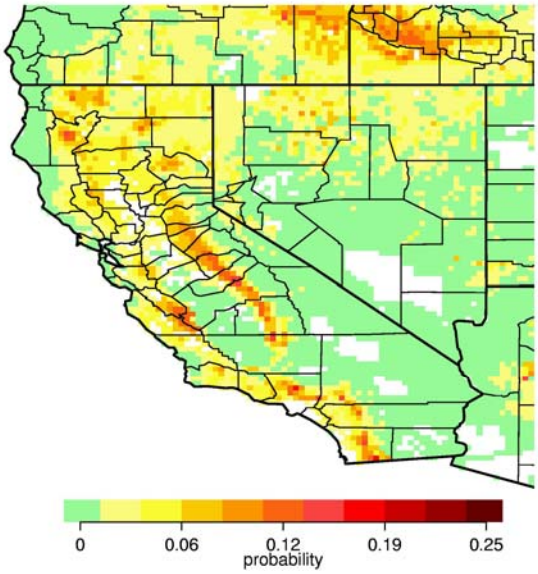

Figure 13. B1 GFDL estimated average annual probabilities of at least one fire > 200 hectares for 1961-1990, 2005-2034, 2035-2064, 2070-2099.

B1 PCM 1961-1990

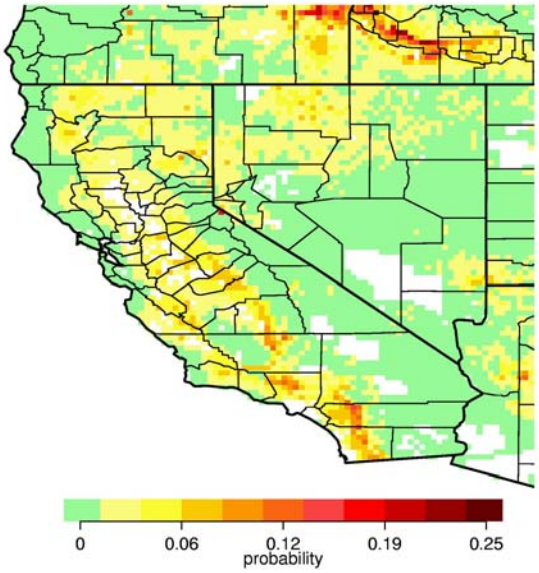

B1 PCM 2005-2034

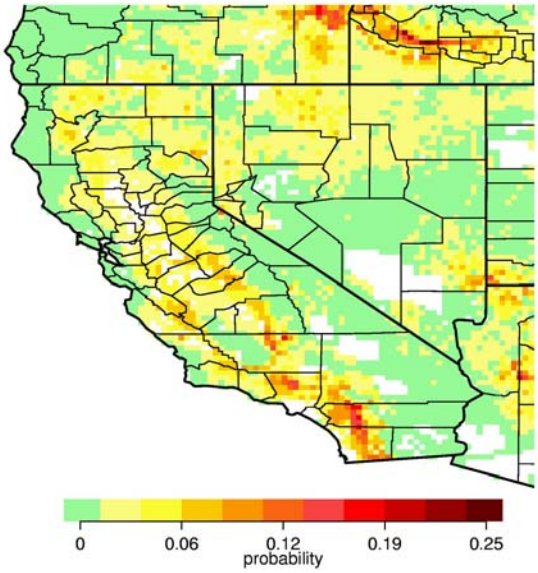

B1 PCM 2035-2064

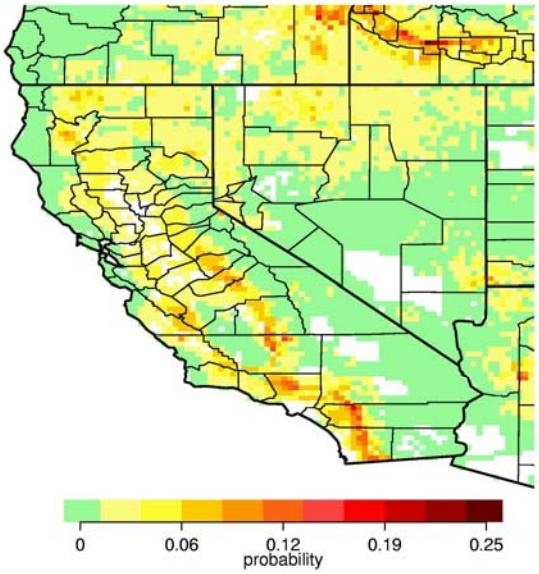

B1 PCM 2070 - 2099

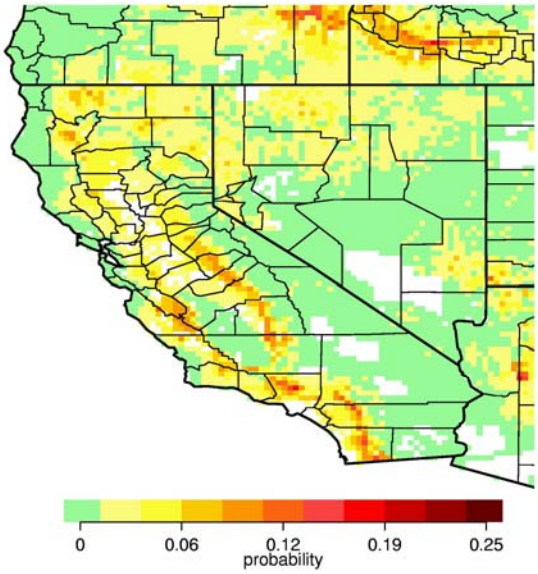

Figure 14. B1 PCM estimated average annual probabilities of at least one fire > 200 hectares for 1961-1990, 2005-2034, 2035-2064, 2070-2099.

A2 GFDL 2070-99 minus 1961-90

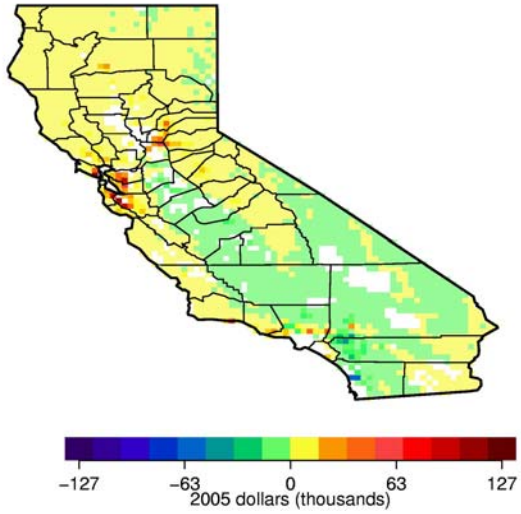

A2 PCM 2070-99 minus 1961-90

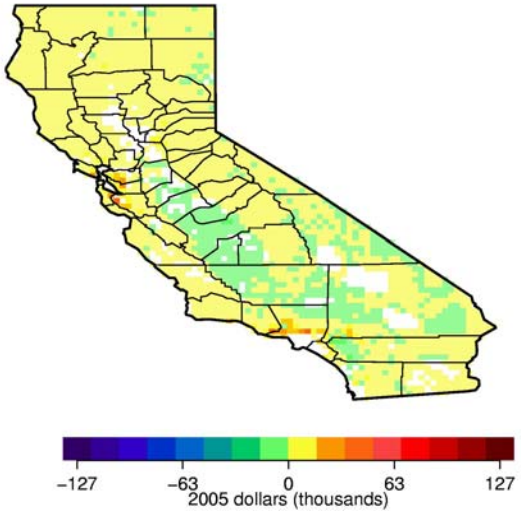

B1 GFDL 2070-99 minus 1961-90

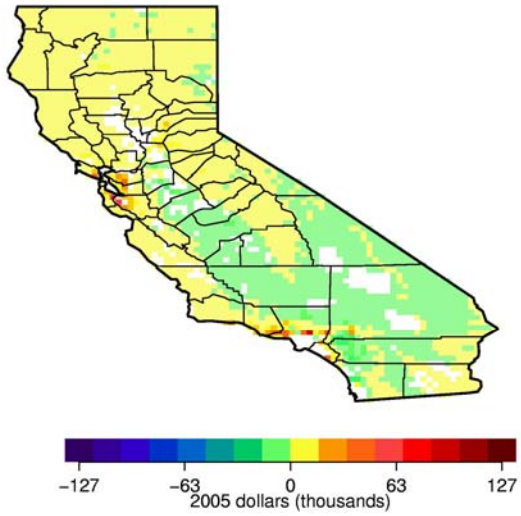

B1 PCM 2070-99 minus 1961-90

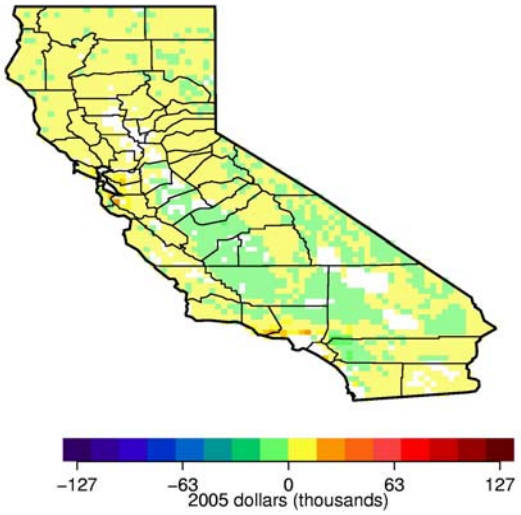

Figure 15. Difference (2070-2099 minus 1961-1990) in estimated average annual property damages due to a single fire = 200 hectares for A2 and B1 emissions scenarios for GFDL and PCM models. This represents the expected damages for the minimum number of fires expected per year.

Table 1. Percentage change in values, structures and fires, 2070-2099 over 1961-1990

	B1 PCM	B1 GFDL	A2 PCM	A2 GFDL
CA Burned Value	15	30	30	36
CA Burned Structures	6	11	21	16
CA Threatened Structures	7	12	21	11
CA Large Fires	12	23	34	53
NC Burned Value	21	48	37	96
NC Burned Structures	12	31	26	75
NC Threatened Structures	12	30	25	71
NC Large Fires	15	38	37	90
SC Burned Value	-6	-10	2	-3
SC Burned Structures	-14	-26	-9	-25
SC Threatened Structures	-14	-26	-9	-25
SC Large Fires	6	-11	28	-29

Table 2: Percentage change in values, structures and fires, 2035-64 over 1961-90

	B1 PCM	B1 GFDL	A2 PCM	A2 GFDL
CA Burned Value	8	21	13	32
CA Burned Structures	5	9	7	20
CA Threatened Structures	4	11	7	20
CA Large Fires	9	15	15	34
NC Burned Value	8	32	17	45
NC Burned Structures	4	20	10	34
NC Threatened Structures	3	19	9	32
NC Large Fires	9	24	16	46
SC Burned Value	-4	-5	-5	2
SC Burned Structures	-7	-17	-13	-12
SC Threatened Structures	-7	-17	-13	-12
SC Large Fires	9	-4	12	9

Table 3: Percentage change in values, structures and fires, 2005-34 over 1961-90

	B1 PCM	B1 GFDL	A2 PCM	A2 GFDL
CA Burned Value	13	15	7	16
CA Burned Structures	14	8	5	7
CA Threatened Structures	13	8	5	8
CA Large Fires	15	13	8	13
NC Burned Value	7	20	6	24
NC Burned Structures	6	14	2	16
NC Threatened Structures	6	13	2	15
NC Large Fires	8	17	6	21
SC Burned Value	5	-1	-6	-3
SC Burned Structures	4	-10	-9	-13
SC Threatened Structures	4	-10	-9	-14
SC Large Fires	30	2	11	-4